CLAY BLOCK PRISMS UNDER COMPRESSIVE LOADS: TESTING AND MODELLING

Ramalho, Marcio Antonio[1]; Taliercio, Alberto[2]

[1] Professor, School of Engineering of S.Carlos, University of S.Paulo, ramalho@sc.usp.br

[2] Professor, Politecnico di Milano, Italy, alberto.taliercio@polimi.it

This paper presents a comparison between the results of experimental and numerical analyses of clay block prisms under compression loads. The main goal of the study is to simulate the nonlinear mechanical response of the prisms, based on the behaviour of blocks and mortar joints, using a numerical non-local damage model specifically developed for quasi-brittle materials. An experimental program, with simple compression tests with displacement control, was carried out to determine the damage parameters for the individual components to characterize the numerical model. Prisms were also tested in simple compression to obtain their complete load-displacement diagrams to failure. Despite the simplicity of the experimental procedure, the obtained results show that the damage model employed is able to predict the strength of the prisms reasonably well, as well as their behaviour in the softening regime.

Keywords: *masonry; compression; testing; damage, finite element*

INTRODUCTION

Damage numerical models can be really important to predict the non-linear behavior of some structural elements. When brittle materials are dealt with, damage-based procedures may be indispensable to simulate the loss of rigidity of the medium due to micro-cracks formation, which can lead it to failure. Kachanov 1958 was probably the first who introduced the damage concept as it is currently known. Another important contribution can be ascribed to Rabotnov 1969, who proposed a damage variable that could be used to reduce the initial rigidity and the strength of the material. Recently, after the formalization of the so-called Continuum Damage Mechanics (Lemaitre and Chaboche 1985), the development of this research field was dramatically quick and widespread. It is noteworthy that for this study the damage mechanics applied to brittle materials, such as structural masonry, is especially important.

About the importance of the study presented here, it is worth highlighting that some codes estimate the structural masonry strength according to tests on prisms. Therefore, the numerical prediction of the prism behavior based on the behavior of its components, units and mortar, is a very interesting way to obtain important information about the masonry behavior itself. Obviously, if this information is obtained based on experimental results carried out only on the masonry components, this procedure will entail a significant saving of time and money.

EXPERIMENTAL PROGRAM

The experimental program was accomplished at the Department of Structural Engineering of University of São Paulo (USP). The tests were carried out both on masonry components, blocks and mortar specimens, and on two-block prisms built with the same components.

The hollow clay blocks had a nominal strength of 6 MPa and the dimensions were 140 × 190 × 390 mm (width × height × length), Figure 1a. The cylindrical mortar specimens had a radius of 50 mm and a height of 100 mm, Figure 1b. Two mortar mix proportions, in volume, were considered: 1:0.5:4.5 (Type ii of BS 5628 1992) and 1:1:6 (Type iii of BS 5628 1992).

(a) Clay Blocks

(b) Mortar specimens

Figure 1: Clay blocks and mortar specimens

All the axial compression tests for components and prisms were performed in order to obtain the complete force-displacement curve for the specimens, that is, the behavior of the specimens from the initial loading stage until the complete failure of the material. Therefore, a hydraulic servo-controlled press under displacement control at 1 μm/s was used. Despite the fact that the press had an internal displacement control, four additional devices for displacement measurement (LVDT) were also used in all the performed tests, see Figure 2.

(a) Block

(b) Mortar specimen

(c) Prism

Figure 2: Axial compression tests

In order to characterize the units, nine clay blocks were tested. From the obtained load-displacement diagrams it was possible to define a representative behavior for the units. Figure 3 summarizes all the results obtained for the prisms and the adopted block diagram that will be used for all the numerical prism models, as described in details in a following section.

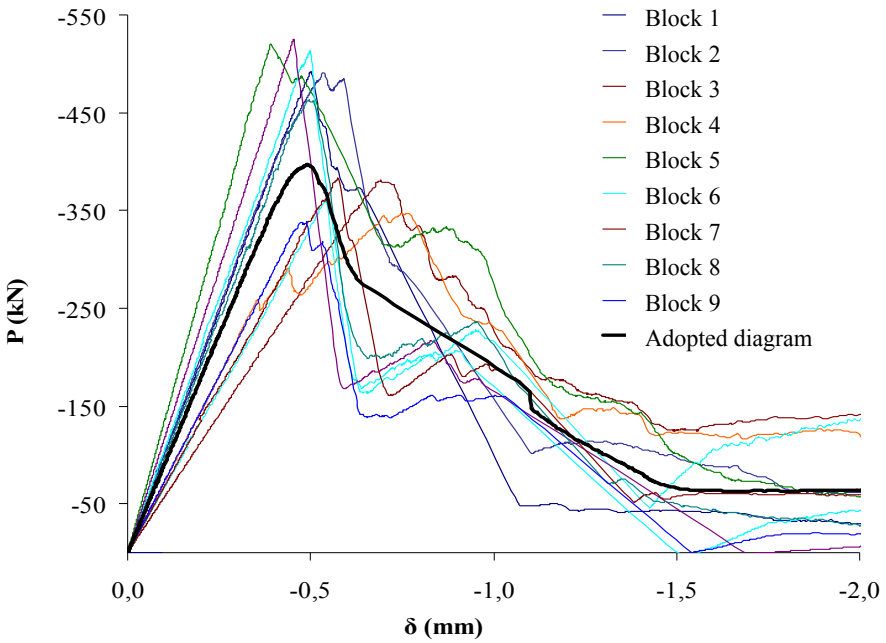

Figure 3: Load-displacement diagrams for the units.

Six prisms were tested under axial compression. Three of them were built using the BS 5628 type ii mortar and the other one with the type iii mortar. For all of the prisms the mortar bed joint was 10 mm thick. The complete load-displacement diagrams were obtained for all the prisms to facilitate the comparison with those obtained numerically. The obtained diagrams are presented in a following section, where the numerical results are compared with the experimental ones.

It is worth noting that for each tested prism a mortar specimen was taken, and considered to be representative of the prism mortar joint. Each of these specimens was also tested to obtain the complete load-displacement diagram. These diagrams will be used to identify the damage parameters for the mortar, as will be seen in detail in a following section. In fact, the cylindrical mortar specimen prepared in a steel mould does not capture the in-situ properties of the mortar bed joint. However, this type of procedure was adopted because it is a standard one: the purposes of the present research project include the validation of the proposed procedure according only to standard tests on the masonry components.

DAMAGE MODEL

The numerical analysis performed in the present paper is based on a damage model originally developed by Papa and Taliercio 2005. This model was adapted by Ramalho et. al. 2005 and implemented in the FEAP® program (FEAP 2002). The obtained local damage procedure is reliable and efficient to evaluate the stress-strain behavior from the initial loading stage until the peak load of any structural element, especially when it is submitted to loadings in which compression is the main effect, Anzani et. al. 2005.

When applied to brittle materials subjected to non-uniform strain, however, the numerical local damage model employed within a finite element program usually leads to strong strain localizations. Spurious results and strong mesh sensitivity are obtained (Jirásek 1998).

Typically, the inelastic strains are localized in an element or in narrow bands of elements, whereas the major part of the structure is nearly unstrained. As a consequence, it is impossible to evaluate the load-displacement diagram correctly, especially in the softening region, i.e. from the peak load to the complete failure of the material element.

Because of these numerical problems, the damage model was modified, and a non-local damage model based on a strain averaging procedure was implemented. In this case, the strain at each point is replaced by a weighted average over a spatial neighborhood of the point (Ramalho et al. 2007).

Discussing in detail the damage model used in the numerical analysis is not the main goal of this paper. Nevertheless, the main characteristics of the model are briefly outlined to make the paper self-contained. Hence, it is important to mention that the damage phenomena are macroscopically taken into account through a symmetric, second-order tensor D. In finite form, the nonlinear stress-strain law of the material reads:

$$\boldsymbol{\varepsilon} = \boldsymbol{C}(\boldsymbol{D})\,\boldsymbol{\sigma} \tag{1}$$

where $\boldsymbol{C}(\boldsymbol{D})$ is the fourth-order flexibility matrix of the damaged material that depends on the damage tensor $\boldsymbol{D}$.

The eigenvalues and the normalized eigenvectors of the damage tensor will be denoted by D_α and n_α (α = I, II, III), respectively. Any one of the planes of damage-induced orthotropy is somehow associated to a plane micro-crack that forms in the solid. Once any damage direction is activated, its orientation is supposed to remain fixed throughout the rest of the stress history.

The damage process driving variable is supposed to be an equivalent strain measure, $\boldsymbol{y} = \tfrac{1}{2}\,\boldsymbol{\varepsilon}^2$. As the maximum eigenvalue of $\boldsymbol{y}$ attains a critical value (y_{0T} or y_{0C}, according to the sign of the associated strain), the first damage direction (n_I) is activated. An additional damage direction, n_II, can be activated in the plane orthogonal to n_I if the maximum direct component of $\boldsymbol{y}$, that is, $y_{hh} = \boldsymbol{n}_\mathrm{h}\cdot(\boldsymbol{y}\cdot\boldsymbol{n}_h)$, with $\boldsymbol{n}_h \perp \boldsymbol{n}_\mathrm{I}$, attains the damage threshold. The third possible damage direction is necessarily $\boldsymbol{n}_\mathrm{III} = \boldsymbol{n}_\mathrm{I} \wedge \boldsymbol{n}_\mathrm{II}$.

Neglecting creep-induced damage, each principal value of the damage tensor is supposed to evolve according to a law of the form:

$$D_\alpha = 1 - \frac{C_H}{1 + A_H \left\langle y_{hh} - y_{0H} \right\rangle^{B_H}},\ \alpha = \mathrm{I, II, III} \tag{2}$$

Here, $\langle * \rangle$ are McAuley brackets and A_H, B_H and C_H are material parameters, which take different values according to the sign of the strain component that activates damage (H=T for tension; H=C for compression).

It is worth mentioning that in the initial stage of the loading, before any damage direction is activated, the material is elastic-linear and isotropic; its behavior is defined by a Young's modulus and a Poisson's ratio.

In addition to the local damage parameters, a suitable spatial neighborhood of any point has to be defined, on which the non-local damage procedure depends. This spatial region is usually a sphere, characterized by its radius. In this paper this radius is adopted as the smallest value for which the numeral procedure is free from strain localization, i.e. mesh dependency effects.

Basically, there are two events indicating the occurrence of strain localization in the analysis. First, the load-displacement diagram presents a clear discontinuity just after the peak load. Second, the number of iterations increases suddenly for the load step just after the load peak; sometimes it is not even possible to attain convergence. Conversely, if the strain concentration phenomenon does not arise, the load-displacement plot does not exhibit any discontinuity and there is not any significant difference in terms of number of iterations in the different load steps of the analysis.

DAMAGE PARAMETERS

Initially, finite element meshes were assembled for the clay block and the mortar specimens, Figure 4. Displacements were restrained along the three cartesian axes, both at the top and at the bottom of the meshes; the displacements that simulated the test loading scheme were applied along the Z axis at the top of the models. Four-node tetrahedra were adopted for the mortar specimens meshes, whereas eight-noded hexahedra were used for the block mesh. The number of elements was 663 and 928 for the mortar specimens and for the block, respectively.

The Young's modulus (E) and the Poisson's ratio (ν) were directly estimated from to the tests carried out on every component. The damage parameters A_c, B_c and C_c, see Equation 2, were identified so as to best fit the experimental load-displacement plot obtained for each component by the numerical curve. Note that for the block the single diagram shown in Figure 3 was adopted, whereas each of the six mortar specimens was characterized by its own diagram.

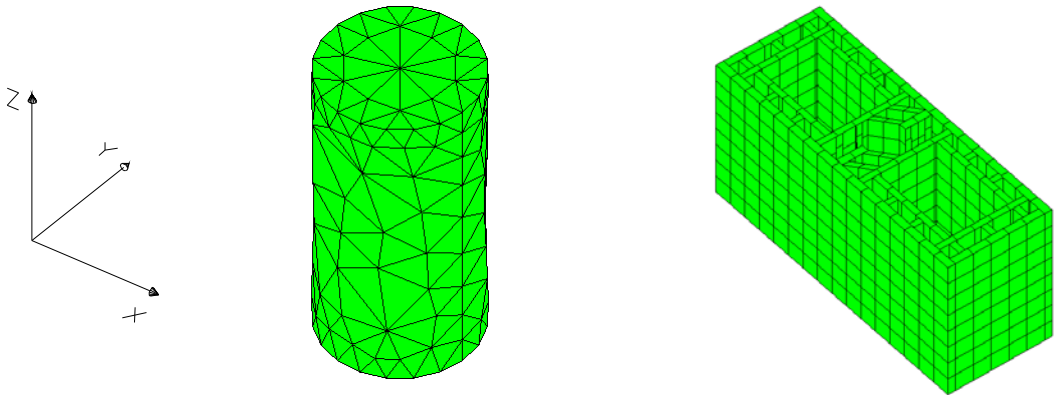

(a) Mortar specimen (b) Block

Figure 4: Finite element meshes.

After assessing the local damage parameters, it was possible to evaluate the spatial neighborhood radius (r_{nl}) to be considered in the non-local damage analyses. As previously

described, in this paper this radius was considered as the smallest value for which no strain localization arises in the numeral procedure.

Table 1 summarizes the values of the parameters obtained for the block and the mortars used to build the prisms. It is relevant to mention that the mortars M1, M2 and M3 could be classified as type ii and the mortars M4, M5 and M5 were type iii (BS 5628 1992), where "Mi" denotes the mortar specimen representative of the bed joint of i-th the prism.

Table 1: Damage parameters for components.

Parameter	Block	Mortar					
		M1	M2	M3	M4	M5	M6
E (N/mm^2)	6574.80	2733.3	4048.7	5733.6	4427.4	3941.3	4530.0
A_c	1.10×10^6	790	375	215	320	315	215
B_c	2.80	0.90	0.83	0.75	0.90	0.85	0.75
C_c	0.97	2.60	1.70	1.50	0.90	1.10	1.10
r_{nl} (mm)	50						
ν	0,20						

The experimental and numerical load-displacement plots for the block are shown in Figure 5, whereas Figures 6a-f show the results for the six mortars specimens. The numerical diagrams were obtained using the parameters shown in Table 1, thaty will be used to model the prisms presented in the following section.

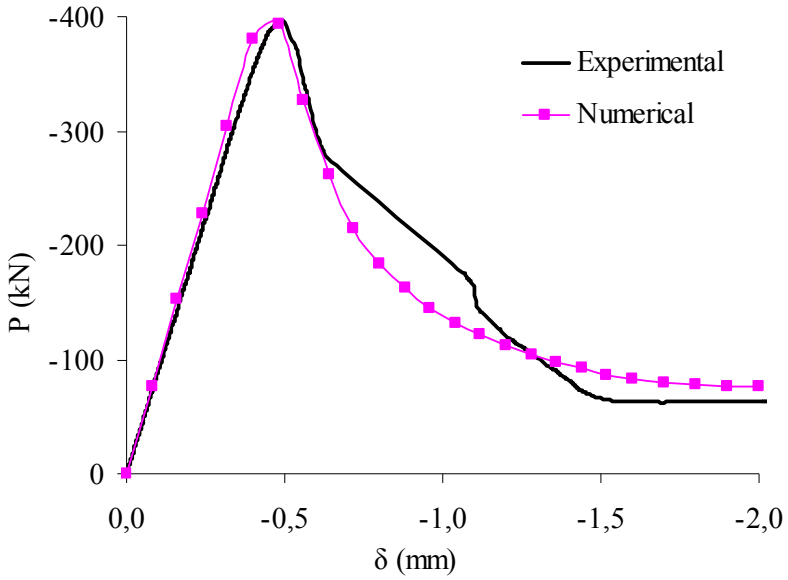

Figure 5: Load-displacement diagram for the block.

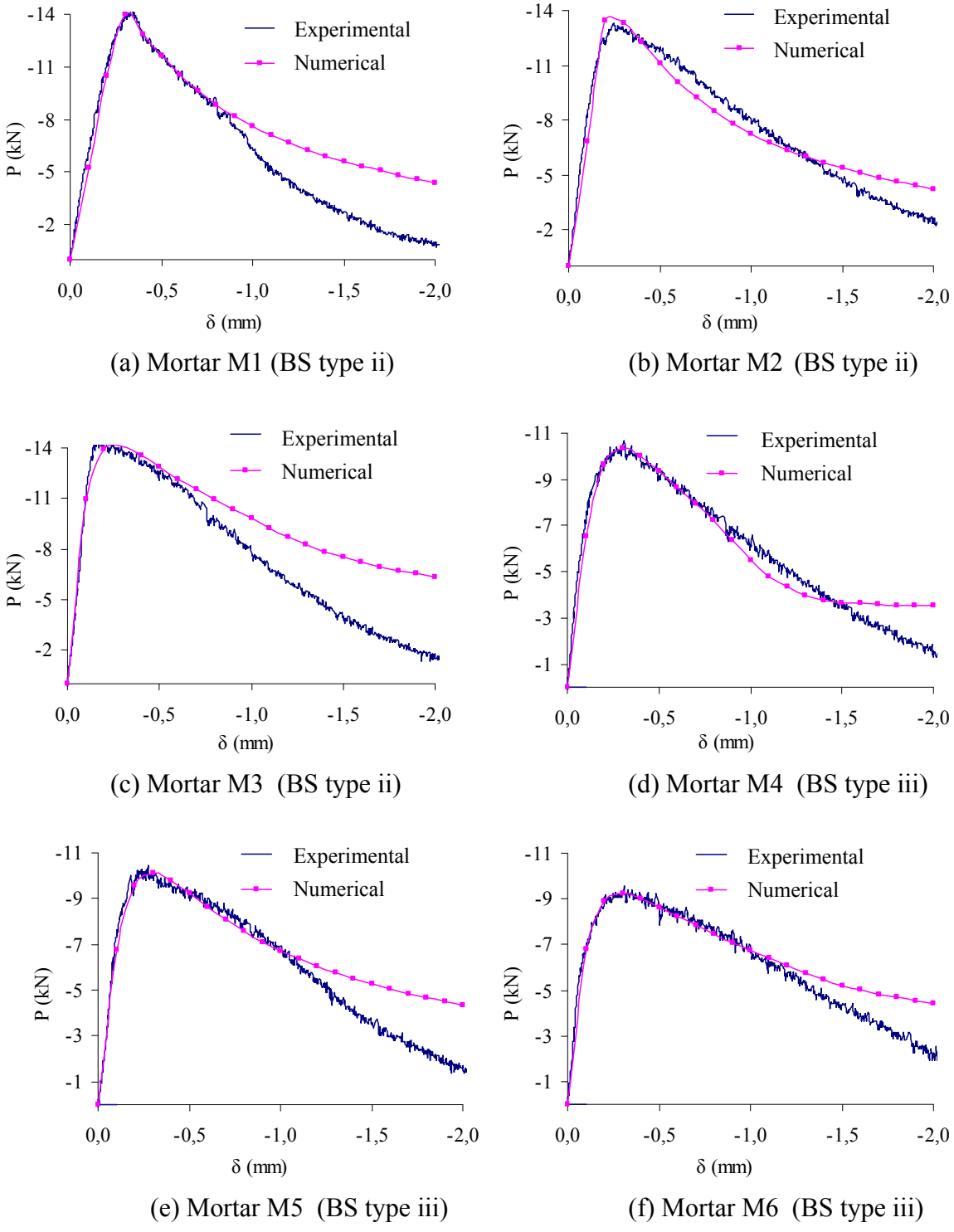

(a) Mortar M1 (BS type ii)

(b) Mortar M2 (BS type ii)

(c) Mortar M3 (BS type ii)

(d) Mortar M4 (BS type iii)

(e) Mortar M5 (BS type iii)

(f) Mortar M6 (BS type iii)

Figure 6: Load-displacement diagrams for the mortars

RESULTS OBTAINED FOR THE PRISMS

The assembled mesh for the prisms had 1972 eight-node hexahedral finite elements and is shown in Figure 7. The parameters shown in Table 1 for the block and the respective mortar

were used to model each prism. Similarly to the models of the mortar specimen and the block, displacements were restrained along the *X*, *Y* and *Z* axes, both at the top and at the bottom of the meshes; an increasing displacement along *Z* was prescribed at the top of the model to simulate the test loading scheme.

In Table 2 the experimental and numerical peak loads are summarized and compared. On the whole, the agreement is satisfactory: the highest discrepancy is obtained for prism P3, for which the numerical peak load overestimates the experimental one by 27.9%. For prism P1 the two values are almost identical, with the experimental value greater only by 3.5% than the numerical peak load.

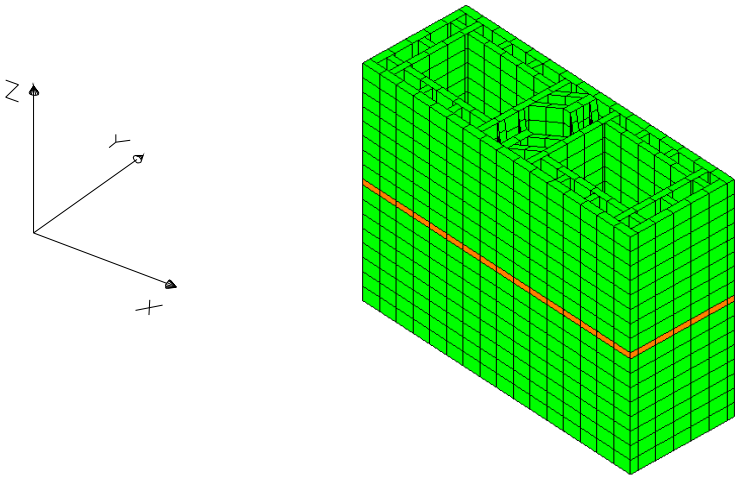

Figure 7: Finite element mesh for the prisms.

Table 2: Maximum load for prisms (kN).

	Prism					
	P1	P2	P3	P4	P5	P6
Experimental	255.76	191.13	192.11	207.38	181.83	233.48
Numerical	246.80	236.54	245.65	223.54	221.58	216.89
Difference (%)	-3.5	23.8	27.9	7.8	21.9	-7.1

Another significant point to be highlighted is the trend of the obtained load-displacement diagram from the initial loading stages until the complete failure of the prisms. In Figure 8 the experimental and numerical plots obtained for the six tested prisms are shown. It is possible to deduce that the trend of the numerical and experimental diagrams is similar for all the prisms. For some of them, for instance prisms P1, P2 and P6, also the displacement at the peak load is accurately predicted by the numerical model.

Finally, it can be noted that the numerical plots are nearly coincident in the linear-elastic stage, despite the different values of the Young's modulus for the mortars, Figure 8. Thus, this parameter does not seem to affect significantly the obtained results, probably due to the small ratio of the bed joint thickness to the block height. After the peak load, however, the numerical plots differ significantly because of the damage activation.

CONCLUSIONS

The main conclusion of this work is that considering only the damage parameters obtained by means of experimental tests on the individual components of masonry prisms, i.e. blocks and mortars, it was possible to numerically predict the behavior of the prisms under compression with good accuracy.

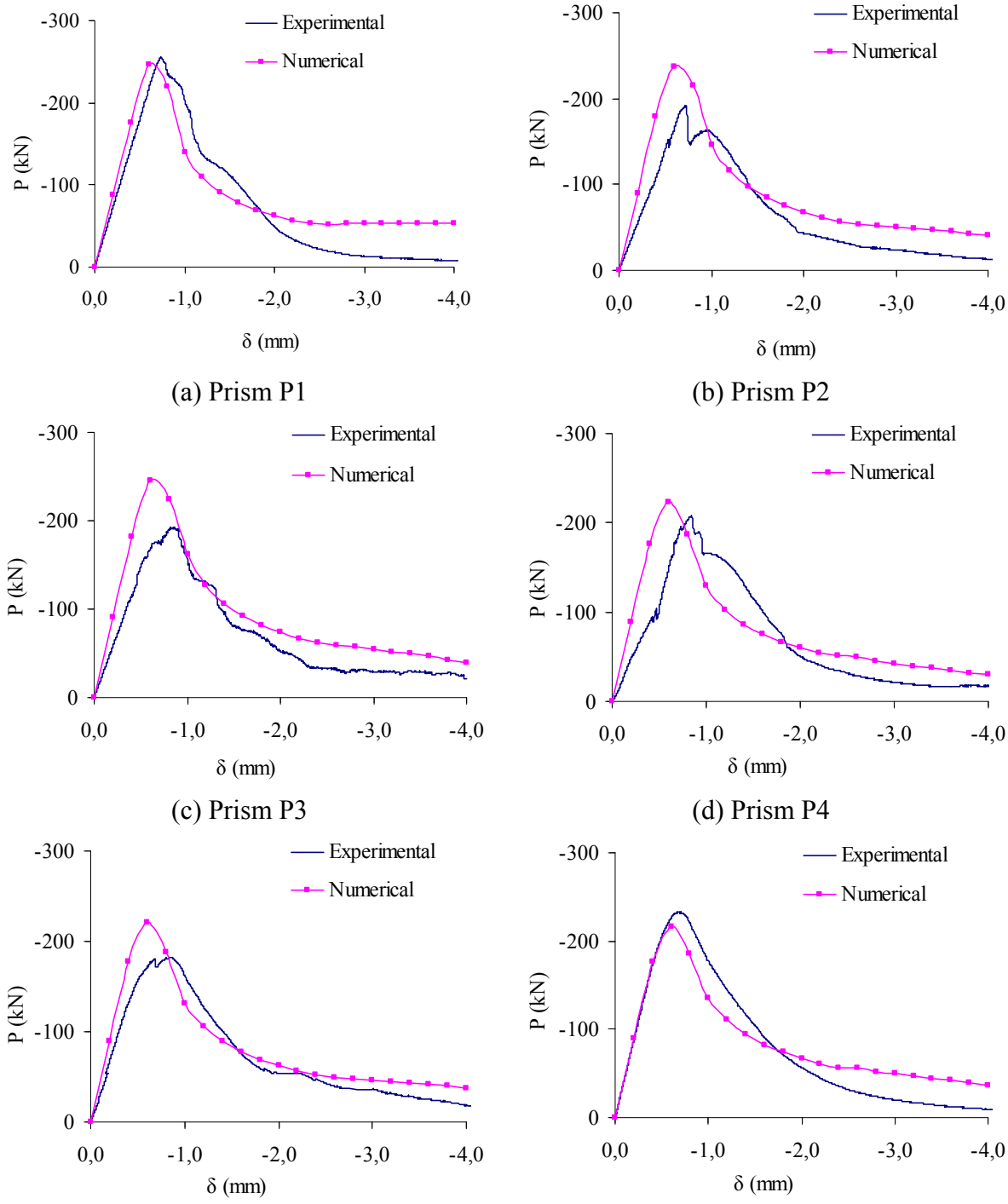

(a) Prism P1 (b) Prism P2

(c) Prism P3 (d) Prism P4

(e) Prism P5 (f) Prism P6

Figure 8: Numerical and experimental load-displacement diagrams for the prisms.

Actually, the non-local numerical model employed is capable to predict different stages of the load-displacement diagram, from the linear-elastic stage until the complete failure of the material element. In particular, the maximum compression load and the relevant displacement can be evaluated fair accuracy, showing that the proposed numerical procedure is efficient and reliable to model structural masonry elements under compression.

According to the obtained results, the numerical procedure proposed can be effectively used to evaluate the strength of any structural masonry element, provided that the mechanical behavior of the block and the mortar is known.

ACKNOWLEDGMENTS

The authors gratefully acknowledge Alexandre Freitas for the experimental results and the support of FAPESP - São Paulo State Research Support Foundation and CNPq – National Council for Scientific and Technological Development.

REFERENCES

Anzani, A.; Binda, L.; Ramalho, M.A.; Taliercio, A., "Historic multi-leaf Masonry walls: experimental and numerical research", *Masonry International*, Vol. 18, No. 3, 2005, pp. 101-114.

BS 5628 "Code of practice for structural use of masonry – Part1: Structural use of reinforced masonry", *British Standard Institution*, London, 1992.

Jirásek, M., "Nonlocal models for damage and fracture: comparison of approaches", *International Journal of Solids and Structures*, Vol. 35, 1998, pp. 4133–4145.

Kachanov, L.M., "Time of the rupture process of non-linear solid mechanics", *Otd. Tech. Nauk*, Vol. 8, 1958, pp. 28-31.

Lemaitre, J.; Chaboche, J.L., "Mechanics of solid materials", *Cambridge University Press*, 1985.

Papa, E.; Taliercio, A., "A damage model for brittle materials under non-proportional monotonic and sustained stresses", *International Journal for Numerical and Analytical Methods in Geomechanics*, Vol. 29, No. 3, 2005, pp. 287-310.

Rabotnov, Y.N., "Creep problems in structural members", *Amsterdam North-Holland*, 1969.

Ramalho, M.A.; Papa, E.; Taliercio, A.; Binda, L., "A Numerical Model for Multi-Leaf Stone Masonry", *Proc. 11th Int. Conf. on Fracture* (ICF-11), Turin (I), March 20-25, 2005, paper no. 5126 (CD–ROM).

Ramalho, M.A.; Taliercio, A.; Anzani, A.; Binda, L.; Papa, E., "A Numerical Model for the Description of the Nonlinear Behaviour of Multi-Leaf Masonry Walls", *Advances in Engineering Software*, Vol. 39, No. 4, 2008, pp. 249–257.